Advances in Applied Mathematics and Mechanics
Adv. Appl. Math. Mech., Vol. **3**, No. 6, pp. 729-744

DOI: 10.4208/aamm.10-m1070
December 2011

Algebraic Multigrid Preconditioning for Finite Element Solution of Inhomogeneous Elastic Inclusion Problems in Articular Cartilage

Zhengzheng Hu and Mansoor A Haider*

Department of Mathematics, North Carolina State University, Box 8205, Raleigh, NC 27695, USA

Received 10 December 2010; Accepted (in revised version) 17 May 2011

Available online 31 October 2011

Abstract. In studying biomechanical deformation in articular cartilage, the presence of cells (chondrocytes) necessitates the consideration of inhomogeneous elasticity problems in which cells are idealized as soft inclusions within a stiff extracellular matrix. An analytical solution of a soft inclusion problem is derived and used to evaluate iterative numerical solutions of the associated linear algebraic system based on discretization via the finite element method, and use of an iterative conjugate gradient method with algebraic multigrid preconditioning (AMG-PCG). Accuracy and efficiency of the AMG-PCG algorithm is compared to two other conjugate gradient algorithms with diagonal preconditioning (DS-PCG) or a modified incomplete LU decomposition (Euclid-PCG) based on comparison to the analytical solution. While all three algorithms are shown to be accurate, the AMG-PCG algorithm is demonstrated to provide significant savings in CPU time as the number of nodal unknowns is increased. In contrast to the other two algorithms, the AMG-PCG algorithm also exhibits little sensitivity of CPU time and number of iterations to variations in material properties that are known to significantly affect model variables. Results demonstrate the benefits of algebraic multigrid preconditioners for the iterative solution of assembled linear systems based on finite element modeling of soft elastic inclusion problems and may be particularly advantageous for large scale problems with many nodal unknowns.

AMS subject classifications: 92C10, 74B05, 65M55

Key words: Biomechanics, interface problem, conjugate gradient method.

1 Introduction

Biomechanical deformation of articular cartilage, the primary load-bearing soft tissue

*Corresponding author.
URL: `http://www4.ncsu.edu/~mahaider/`
Email: zhu4@ncsu.edu (Z. Z. Hu), m_haider@ncsu.edu (M. A. Haider)

in joints such as the knee, shoulder and hip, is commonly modeled via biphasic continuum mixture theories [16] that idealize the tissue as a fluid-saturated porous medium. In compressive loading at mechanical equilibrium, biphasic deformation of articular cartilage can be modeled based on elasticity theory. However, the presence of a single, sparsely distributed, population of cells (chondrocytes) necessitates the consideration of inhomogeneous inclusion problems in which each cell is idealized as a soft inclusion within a stiff extracellular matrix. Simulating inhomogeneous deformation in the biomechanical microenvironment of the cells in articular cartilage is challenging due to coupled effects among these distinct cartilage regions as they also span disparate length scales (μm to mm), and a wide range of elastic stiffness (KPa to Mpa).

To date, several numerical methods have been developed to study interface problems that exhibit inhomogeneous elastic deformation. For example, in [15], an axisymmetric boundary element method (BEM) for linear elastic domains with internal interfaces was developed. Using direct methods to solve the associated linear algebraic system, the BEM was used to determine linear elastic properties of a pericellular matrix surrounding individual cells via inverse analysis of previously reported experimental data for in situ cell deformation within a cylindrical cartilage explant under static compression. Z. Li and co-authors [6, 7] developed a new immersed interface finite element method to capture the jump conditions along an internal interface for structured meshes. Due to their versatility in generation of unstructured meshes (e.g., via triangular or tetrahedral elements), finite element methods are most commonly used to model elastic deformation in the presence of curved internal interfaces. Use of iterative methods, such as Krylov subspace methods [19], for solution of the assembled linear algebraic systems ensures scalability to problems of moderate to large scale. However, it is well known that the convergence rate of an iterative method depends strongly on the spectral properties of associated operators and, as such, accuracy and efficiency of the associated numerical solutions depend on the choice of algorithm.

Multigrid (MG) methods can be used to significantly accelerate the convergence of iterative methods [2, 20]. When they are well-suited to an application, MG methods exhibit convergence that is independent of problem size [9]. Success of MG techniques is rooted in the differing convergence rates of errors on coarse versus fine grids that are captured by "V-cycles" that traverse the coarse and fine grids during the iterative solution procedure. While initially considered for classical scalar elliptic PDEs, MG methods were later extended to systems of PDEs. Whereas geometric multigrid (GMG) methods require the use of structured hierarchical meshes, algebraic multigrid (AMG) methods effectively induce coarse discretization via direct indexing within the linear algebraic system. Some AMG studies of linear elasticity on unstructured grids relevant to the current work are those of Griebel et al. [8] and Xiao et al. [17], and both studies iterate over multiple V-cycles. In [8], equations of 2D and 3D linear isotropic elasticity were considered and analysis of a blockwise generalization of an AMG method [18] was performed, demonstrating convergence rates independent of problem size. In [17], Xiao et al. considered 2D elastic domains with highly dis-

continuous values for the Young's modulus and, in one of their numerical examples, considered a square domain with a circular inclusion. Emphasis was placed on comparing scalar-based AMG methods to two new methods based on coarsening with alignment of coarse grid nodes to the internal interface. In the same study they also developed a second method, with improved performance, that utilized a block Gauss-Seidel smoother where the blocks were exclusive to regions in, or on opposite sides of, the internal interface. While both methods performed substantially better than scalar-based AMG methods, the number of AMG iterations for the case of the circular inclusion was dependent on problem size, and increased significantly as the Young's modulus of the circular inclusion was increased to 100 times that of the exterior region.

In the current study, our focus is on demonstrating the accuracy, efficiency and scalability of a numerical approach that combines an iterative conjugate gradient solution technique with use of AMG as a preconditioner (AMG-PCG) in the context of a finite element discretization with conforming triangular elements. To facilitate this analysis, an analytical solution of a soft inclusion problem motivated by the biomechanical deformation of cells in articular cartilage is derived. The resulting analytical solution is then used to evaluate accuracy and efficiency of the AMG-PCG algorithm by comparison to similar methods with two other, commonly used, preconditioners. Sensitivity of algorithm performance is also evaluated by varying material properties in ranges representative of articular cartilage and spatial distributions of error are also determined to evaluate and compare performance of the three algorithms.

2 Model and analytical solution

2.1 Governing equations

Biomechanical deformation in the cellular microenvironment of articular cartilage is commonly modeled by idealizing the tissue as a biphasic continuum mixture [16] comprised of a solid phase that is saturated by a second phase of interstitial fluid. Under equilibrated, compressive loading in the range of small strain, fluid motion ceases and the governing equations for biphasic deformation of articular cartilage reduce to those of linear elastostatics. Modeling cell-matrix interactions necessitates the consideration of inhomogeneous inclusion problems in which each cartilage cell (c) is idealized as a soft inclusion within a stiffer region that represents the extracellular matrix (e). For isotropic materials, this motivates consideration of boundary value problems on a domain

$$\overline{\Omega} = \overline{\Omega}_c \cup \overline{\Omega}_e,$$

where

$$\overline{\Omega}_i = \Omega_i \cup \Gamma_i, \quad i = c, e,$$

that are of the form:

$$\nabla \cdot \sigma = \mathbf{0}, \qquad \text{on } \Omega_c \cup \Omega_e, \text{ with } \sigma = \lambda_i \mathrm{tr}(\mathbf{e})\mathbf{I} + 2\mu_i \mathbf{e}, \tag{2.1a}$$

$$\mathbf{u} = \mathbf{f}, \qquad \text{on } \Gamma_e, \tag{2.1b}$$

$$\mathbf{u}^+ = \mathbf{u}^-, \qquad \text{on } \Gamma_c, \tag{2.1c}$$

$$\sigma \cdot \mathbf{n}^+ = \sigma \cdot \mathbf{n}^-, \qquad \text{on } \Gamma_c. \tag{2.1d}$$

In (2.1a)-(2.1b), σ is the Cauchy stress tensor, $\mathbf{e}=\nabla\mathbf{u}+(\nabla\mathbf{u})^T$ is the infinitesimal strain tensor, $\mathbf{u}$ is the displacement, $\mathbf{I}$ is the identity tensor, and λ_i, $\mu_i (i=c,e)$ are solid phase Lamé coefficients associated with the state of "drained" biphasic equilibrium in each of the two sub-domains.

2.2 Radial analytical solution for a circular inclusion

In 2D, there are many well known elementary linear elasticity solutions for a homogeneous domain, e.g., plane strain, plane stress etc. A well known solution for inclusion problems is due to Eshelby [5], but it requires the region outside the inclusion to have infinite extent. For problems with internal interfaces, another technique for evaluating the performance of numerical schemes is to develop analytical solutions involving nonzero body force terms (in Eq. (2.1a)) that are tailored to satisfy the governing equations, see e.g., [6, 17, 22]. However, such an approach does not accurately reflect boundary conditions associated with boundary value problems that model loading conditions for biomechanical inclusion problems, where the body forces are almost always assumed to be zero.

Consequently, we develop a 1D (radial) analytical solution of Eqs. (2.1a)-(2.1d) that more closely reflects the inclusion problem arising for deformation of cells within a finite region representing the extracellular matrix (ECM) of articular cartilage. It is known that these cells are much softer than the ECM $(E_c \ll E_e)$ and are, typically, more incompressible than the ECM $(0 \le \nu_e < \nu_c < 0.5)$, where

$$\lambda_i = \frac{E_i \nu_i}{(1+\nu_i)(1-2\nu_i)} \quad \text{and} \quad \mu_i = \frac{E_i}{2(1+\nu_i)}, \quad i = c, e.$$

To this end, consider a disk of radius b representing the ECM region that contains a soft circular inclusion of radius a modeling the cell (Fig. 1). We build an analytical solution

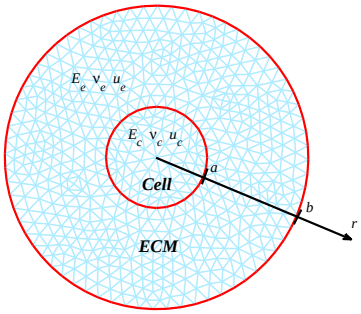

Figure 1: Illustration of conforming mesh of triangular finite elements modeling the geometry of the soft inclusion problem.

to the 2D plane strain inclusion problem using an Airy stress function ϕ ($\nabla^4\phi$=0) in cylindrical coordinates [1] with the following representation:

$$\phi_c = S_1 r^2, \qquad 0 \le r \le a, \tag{2.2a}$$

$$\phi_e = S_2 r^2 + S_3 \ln r, \qquad a \le r \le b, \tag{2.2b}$$

where S_1, S_2 and S_3 are constants to be determined. Assuming purely radial deformation, inversion of the stress-strain relations yields the equation

$$\frac{u^r}{r} = \epsilon_{\theta\theta} = \frac{1+\nu}{E}\left[(1-\nu)\sigma_{\theta\theta} - \nu\sigma_{rr}\right], \tag{2.3}$$

where

$$\sigma_{rr} = \frac{1}{r}\frac{\partial\phi}{\partial r}, \quad \sigma_{\theta\theta} = \frac{\partial^2\phi}{\partial r^2}, \quad \sigma_{r\theta} = 0. \tag{2.4}$$

Substitution of Eqs. (2.2) and (2.4) into Eq. (2.3), yields the displacement solution representation:

$$u^r = \begin{cases} C_1 r, & \text{for } 0 \le r < a, \\ C_2 r - \dfrac{C_3}{r}, & \text{for } a \le r \le b, \end{cases} \tag{2.5a}$$

$$u^\theta = 0, \qquad \text{for } 0 \le r \le b, \tag{2.5b}$$

where C_1, C_2 and C_3 are constants to be determined. Continuity of radial displacement along the interface Γ_c (r=a) yields the constraint C_3=$(C_2 - C_1)a^2$. Using the strain-displacement relations in polar coordinates (assuming purely radial deformation):

$$\epsilon_{rr} = \frac{\partial u^r}{\partial r}, \quad \epsilon_{\theta\theta} = \frac{u^r}{r}. \tag{2.6}$$

Eq. (2.1d) can be expressed as:

$$\begin{aligned} \sigma_{rr}(a^+) =& \sigma_{rr}(a^-) \Rightarrow \left(\lambda_e + 2\mu_e\right)\frac{\partial u^r}{\partial r}(a^+) + \lambda_e\frac{u^r(a^+)}{a} \\ =& \left(\lambda_c + 2\mu_c\right)\frac{\partial u^r}{\partial r}(a^-) + \lambda_c\frac{u^r(a^-)}{a}. \end{aligned} \tag{2.7}$$

Substituting Eq. (2.5) into Eq. (2.7) and simplifying yields the relation:

$$C_2 = \gamma C_1, \quad \text{where } \gamma = \frac{\lambda_c + \mu_c + \mu_e}{\lambda_e + 2\mu_e}. \tag{2.8}$$

In Eq. (2.1b), we consider a boundary condition of the form:

$$u^r(b) = \epsilon b, \tag{2.9}$$

where ϵ is a compressive apparent (engineering) strain. Combining Eqs. (2.5), (2.8) and (2.9) yields the following expressions for the unknown constants in Eq. (2.5):

$$C_1 = \frac{\epsilon b^2}{a^2 + \gamma(b^2 - a^2)}, \quad C_2 = \gamma C_1, \quad C_3 = (\gamma - 1)a^2 C_1. \tag{2.10}$$

Therefore, the analytical displacement solution of Eqs. (2.1a)-(2.1d) is given by:

$$u^r = \begin{cases} C_1 r, & \text{for } 0 \le r < a, \\ C_1\Big(\gamma r - \dfrac{(\gamma-1)a^2}{r}\Big), & \text{for } a \le r \le b, \end{cases} \tag{2.11a}$$

$$u^\theta = 0, \qquad \text{for } 0 \le r \le b. \tag{2.11b}$$

Using Eq. (2.6), the strain components are given by:

$$\epsilon_{rr} = \begin{cases} C_1, & \text{for } 0 \le r < a, \\ C_1\Big(\gamma + \dfrac{(\gamma-1)a^2}{r^2}\Big), & \text{for } a \le r \le b, \end{cases} \tag{2.12a}$$

$$\epsilon_{r\theta} = 0, \qquad \text{for } 0 \le r \le b, \tag{2.12b}$$

$$\epsilon_{\theta\theta} = \begin{cases} C_1, & \text{for } 0 \le r < a, \\ C_1\Big(\gamma - \dfrac{(\gamma-1)a^2}{r^2}\Big), & \text{for } a \le r \le b. \end{cases} \tag{2.12c}$$

Lastly, the stress-strain relations in Eq. (2.1a), give the following stress components:

$$\sigma_{rr} = \begin{cases} 2(\lambda_c + \mu_c)C_1, & \text{for } 0 \le r < a, \\ 2(\lambda_e + \mu_e)\gamma C_1 + \dfrac{2\mu_e(\gamma-1)a^2 C_1}{r^2}, & \text{for } a \le r \le b, \end{cases} \tag{2.13a}$$

$$\sigma_{r\theta} = 0, \qquad \text{for } 0 \le r \le b, \tag{2.13b}$$

$$\sigma_{\theta\theta} = \begin{cases} 2(\lambda_c + \mu_c)C_1, & \text{for } 0 \le r < a, \\ 2(\lambda_e + \mu_e)\gamma C_1 - \dfrac{2\mu_e(\gamma-1)a^2 C_1}{r^2}, & \text{for } a \le r \le b. \end{cases} \tag{2.13c}$$

3 Numerical solution

3.1 Finite element discretization

The Finite Element Method (FEM) has seen wide application in the context of modeling the mechanics of linear elastic solids. Consider Eqs. (2.1a)-(2.1d) on a 2D domain Ω that has been partitioned into P finite elements $\{\Omega_p\}_{p=1}^{P}$ with a total of M nodes. Global assembly based on a standard Galerkin FEM formulation with a Dirichlet boundary condition, i.e., Eq. (2.1b), leads to a discrete system of the form $(i, j{=}1, 2)$:

$$\tilde{K}_{nimj} u_j^m = F_i^n, \quad \text{where } \tilde{K}_{nimj} = \int_\Omega C_{ijkl} \frac{\partial N^n(\mathbf{x})}{\partial x_k} \frac{\partial N^m(\mathbf{x})}{\partial x_l} dS, \ \ m, n = 1, \cdots, M. \tag{3.1}$$

In Eq. (3.1), $\tilde{K}_{nimj}$ is the global stiffness tensor, C_{ijkl} is the elasticity tensor, u_i^n, F_i^n denote the ith displacement and body force components (respectively) at node n, $N^n(\mathbf{x}) \in H^1(\Omega)$ is the shape function at node n and typically has local support in the neighboring elements, and the Einstein summation convention applies to repeated indices. By assembling the nodal displacement components into a column vector $\mathbf{u}$, the global stiffness tensor can be re-written as a global stiffness matrix $\mathbf{K}$, and the reduced form of Eq. (3.1) is then

$$\mathbf{Ku} = \mathbf{0}.$$

Accounting for prescribed (essential) boundary conditions in Eq. (2.1b) at nodes along the domain boundary $\partial\Omega$, a linear algebraic system

$$\mathbf{Ax} = \mathbf{b},$$

is obtained where $\mathbf{x}$ is the column vector of all (unknown) interior nodal displacement components. For inhomogeneous domains with piecewise constant material properties, the use of triangular elements that conform to the *Cell-ECM* interface (e.g., Fig. 1) enforces displacement continuity (Eq. (2.1c)) as well continuity of tractions (Eq. (2.1d)).

3.2 Algebraic multigrid (AMG) method

To efficiently solve the linear algebraic system described above for a large number of unknowns, it is necessary to consider iterative methods as an alternative to direct methods. Multigrid (MG) techniques [2] significantly accelerate iterative solution of discretized elliptic PDEs and, in particular, are well-suited to domains with multiple length scales. The hallmark of MG is transitioning (via the V-cycle) between coarse and fine mesh representations of the domain to, periodically, insert corrections to the iterative solution based on the coarse mesh representations. The resulting MG "acceleration" is based on the property that iterative algorithms exhibit different convergence rates for high and low frequency components of the PDE solution. While many convergence results are known for geometric multigrid (GMG) methods, which are based on structured (e.g., hierarchical rectangular) meshes, GMG can be difficult to apply to domains with curved internal interfaces. Such domains are more easily discretized using unstructured meshes with triangular (2D) (Fig. 1) or tetrahedral (3D) meshes. Algebraic multigrid (AMG) methods provide an alternative approach in which coarsening is defined by a subset of the unknowns and indexed directly in the matrix of the linear algebraic system. AMG methods can employ geometric information to aid in coarsening or operate in a fashion wholly independent of the mesh, e.g., by defining smooth error as that which persists after a few iterations of relaxation.

Often, MG/AMG algorithms iterate on multiple V-cycles and a suitable iterative relaxation scheme is chosen on finer meshes, whereas a direct solver is used at the scale of the coarsest mesh. An alternate approach is to use one AMG V-cycle as a preconditioner that operates within an iterative relaxation scheme. For example, in an AMG Preconditioned Conjugate Gradient method (AMG-PCG), a single AMG V-cycle

serves as the preconditioner through which the solution to

$$\mathbf{Ax} = \mathbf{r},$$

is found, iteratively, where $\mathbf{r}$ is the residual.

In the current study, our focus is on demonstrating the accuracy, efficiency and scalability of an AMG-FEM approach based on the use of the open source software library HYPRE [11] to solve soft circular inclusion problems with highly discontinuous material properties. HYPRE, developed by Lawrence Livermore National Lab, is comprised of high performance preconditioners and iterative solvers for the solution of large, sparse linear systems with capabilities for implementation in parallel computing environments. The library features a parallel algebraic multigrid solver (BoomerAMG) [10,18,21], that is well-suited to linear systems arising from discretization of elliptic PDEs on unstructured grids. In prior work by Henson and Yang [10,21], BoomerAMG was shown to be highly accurate and efficient in solving the 3D Laplace equation using FEM on unstructured grids. While BoomerAMG is capable of parallelization, in the current study, it will be employed in the context of a single processor environment.

4 Results

The 2D boundary value problem associated with the numerical solution described in Section 2.2 was numerically discretized using the FEM described in Section 3.1. We utilized six-node isoparametric quadratic triangular elements that conformed to the boundary Γ_e and the cell-ECM interface Γ_c (Fig. 1). Geometric parameters were fixed at a=10μm, b=30μm, and the apparent (compressive) strain was set at ϵ=−0.05. Numerical solution of the assembled linear algebraic system was implemented within the framework of HYPRE by integrating AMG preconditioning, via BoomerAMG, with the preconditioned conjugate gradient algorithm. All simulations were implemented in C/C++ and performed on an Apple MacPro desktop computer (Dual 2.26 GHz Quad-Core Intel Xeon processors).

BoomerAMG provides a variety of coarsening strategies for the AMG V-cycle as well as several choices for iterative relaxation. We employed Falgout coarsening, which is a hybrid scheme combining Ruge-Stüben (RS) coarsening [10] with Cleary-Luby-Jones-Plassman (CLJP) parallel coarsening [4, 13, 14]. Specifically, in Falgout coarsening, RS is used to coarsen interior regions while CLJP is used to coarsen near boundaries [10]. For iterative relaxation, we used pointwise Gauss-Seidel hybrid relaxation (pointwise Gauss-Seidel on the interior and a Jacobi-like smoother near the boundaries) with Gaussian elimination for solution on the coarsest grid [10,21].

The performance of the Conjugate Gradient Algorithm with AMG preconditioning (AMG-PCG) was compared to two alternative preconditioners: (i) diagonal preconditioning (DS-PCG), and (ii) a modified incomplete LU (ILU(k)) decomposition (Euclid-PCG) [11] with level of fill-in taken as k=0 [12]. In AMG-PCG, the selection of the

Table 1: Values of parameters for all test cases.

case 0	case 1	case 2	case 3	case 4
$E_e = 500$KPa	$E_e = 500$KPa	$E_e = 500, 50, 5$KPa	$E_e = 500$KPa	$E_e = 500$KPa
$E_c = 0.35$KPa	$E_c = 0.35$KPa	$E_c = 0.35$KPa	$E_c = 0.35$KPa	$E_c = 0.35$KPa
$\nu_e = 0.05$	$\nu_e = 0.05, 0.15, 0.25, 0.35$	$\nu_e = 0.05$	$\nu_e = 0.05$	$\nu_e = 0.05$
$\nu_c = 0.45$	$\nu_c = 0.45$	$\nu_c = 0.45$	$\nu_c = 0.45, 0.35, 0.25$	$\nu_c = 0.45$
tol$= 10^{-7}$	tol$= 10^{-7}$	tol$= 10^{-7}$	tol$= 10^{-7}$	tol$= 10^{-7}, 10^{-6}, 10^{-5}$

coarsest mesh was automated in the sense that it was proportional to the logarithm of the total number of nodal unknowns.

In Section 4.1, the accuracy and efficiency of the AMG-PCG strategy is evaluated using the analytical solution and in the context of a baseline case (Table 1, case 0) with material properties that are representative of articular cartilage and a prescribed relative residual tolerance ("tol" in Table 1). In Section 4.2, three other cases (Table 1, cases 1-3) are considered in which several material properties (ν_e, E_e, and ν_c) are varied to assess effects on efficiency of the iterative algorithm with a fixed tolerance. Lastly, in Section 4.3, the spatial distribution of error is compared to demonstrate differences between the three algorithms being considered.

4.1 Case 0: the baseline case

Analytical solutions for the baseline case are illustrated in Fig. 2. To evaluate efficiency, both the iteration counts and the CPU time (in seconds) required to solve the linear algebraic system are reported in Table 2 for the three algorithms considered. We observe that the number of iterations used by AMG-PCG solver does not increase as the number of degrees of freedom (DOF) increases. In contrast, the iteration count for the DS-PCG and the Euclid-PCG algorithms increases dramatically. Since there is significant overhead associated with AMG preconditioning, the associated CPU times were also compared (Table 2). As the number DOF is increased between roughly 9,000-141,000,

Table 2: Iteration counts and CPU time (seconds) for the baseline (case 0, Table 1).

	iteration counts			CPU time (seconds)		
DOF	DS-PCG	Euclid-PCG	AMG-PCG	DS-PCG	Euclid-PCG	AMG-PCG
$N_1 = 2261$	215	79	9	6.48E-2	7.34E-2	6.83E-2
$N_2 = 8905$	418	157	9	5.13E-1	5.89E-1	3.22E-1
$N_3 = 35345$	850	309	9	6.14E+0	4.59E+0	1.62E+0
$N_4 = 140833$	1689	592	9	5.70E+1	4.18E+1	7.78E+0

Table 3: Errors and convergence rates of the radial displacement u^r for the baseline (case 0, Table 1).

	Error in L_∞			Error in L_2		
DOF	DS-PCG	Euclid-PCG	AMG-PCG	DS-PCG	Euclid-PCG	AMG-PCG
$N_1 = 2261$	3.0132E-3	3.0132E-3	3.0146E-3	9.5337E-4	9.5338E-4	9.5336E-4
$N_2 = 8905$	7.0834E-4	7.0834E-4	7.0964E-4	2.3301E-4	2.3302E-4	2.3300E-4
$N_3 = 35345$	1.7137E-4	1.7368E-4	1.6900E-4	5.7917E-5	5.7892E-5	5.7837E-5
$N_4 = 140833$	4.7281E-5	4.6916E-5	4.1281E-5	1.4933E-5	1.4870E-5	1.4576E-5
Rate	2.0029	2.0043	2.0641	1.9998	2.0017	2.0104

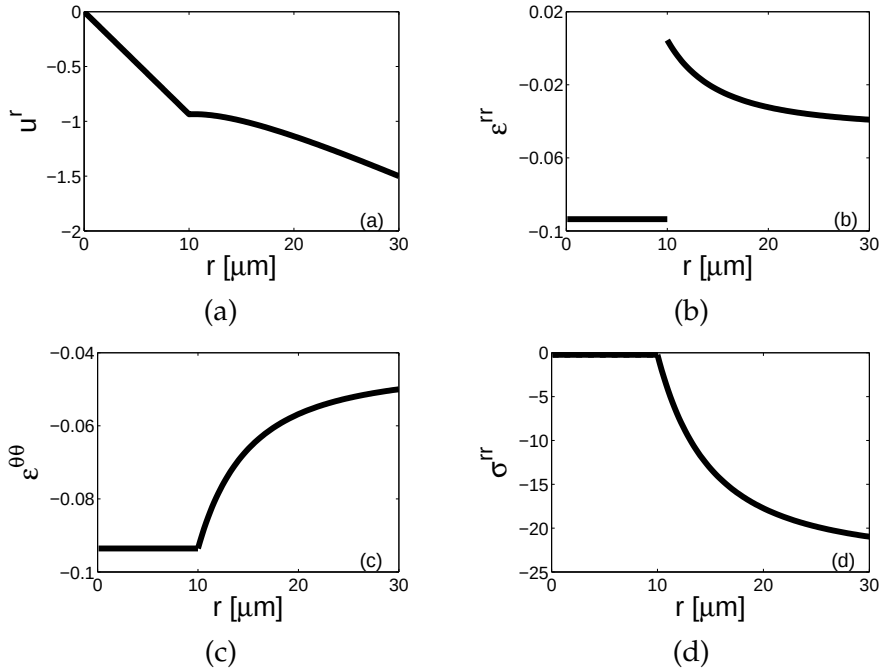

Figure 2: Analytical solutions for the baseline case (case 0, Table 1): (a) radial displacement, (b) radial normal strain, (c) angular normal strain, (d) radial normal stress.

we observe that the AMG-PCG algorithm is 1.8-5.4 times faster than the Euclid-PCG algorithm and 1.6-7.3 times faster than the DS-PCG algorithm.

To assess accuracy, the numerical solution for radial displacement u^r is compared with the analytical solution given in Eq. (2.11b) using both L_∞ and L_2 norms (Table 3). Note that both error norms for u^r were calculated at all nodal points of the triangular elements. In addition, to evaluate the convergence rate, for a given number of DOF the minimum side length of the triangular elements was used to obtain h=1.6μm on the coarsest mesh with $h/2$, $h/4$ and $h/8$, respectively, on the three successively refined

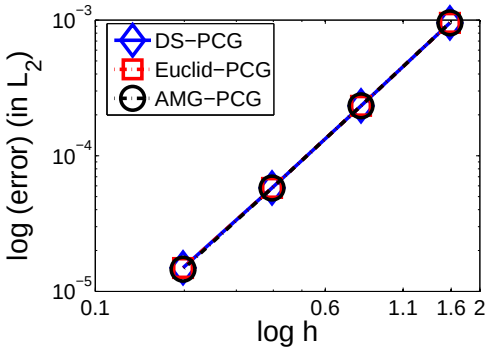

Figure 3: Illustration of effective convergence rate (see Table 3) for the baseline case (case 0, Table 1) using the L_2 norm and the minimum side length (h) of the triangular elements.

meshes. The resulting effective convergence rates for all three algorithms are shown in Table 3 and Fig. 3. Given the tolerance specified in Table 1 (case 0), we observe that all three algorithms exhibit very similar accuracy and convergence rates in both the L_∞ and L_2 norms. We note that our observed convergence rate for quadratic elements (≈ 2), which is strongly affected by the use of a conforming mesh based on triangular elements, could be improved via specialized techniques along the boundary and interface, see e.g., [3,7].

4.2 Sensitivity to material properties

To analyze effects of sensitivity of the solution to variations in material properties on performance of the three algorithms, we consider cases 1-3 (see Table 1). Illustrations of sensitivity of the analytical solution to parameter variations are shown for case 1 (Fig. 4) and case 2 (Fig. 5). We observe high sensitivity of analytical solutions to the variations in ν_e (Fig. 4), and sensitivity to variations in E_e when the extracellular region is highly stiff relative to the cell (Fig. 5). We observe in case 1 (Fig. 4(b)) that, for a stiff extracellular region, the radial strain is tensile near the internal interface, even though the cellular and the prescribed engineering strain $(\epsilon = -0.05)$ are both compressive. Analytical solutions for case 3 are not shown since sensitivity of model variables to variations in ν_c between 0.25 and 0.45 were much less pronounced than for cases 1 and 2.

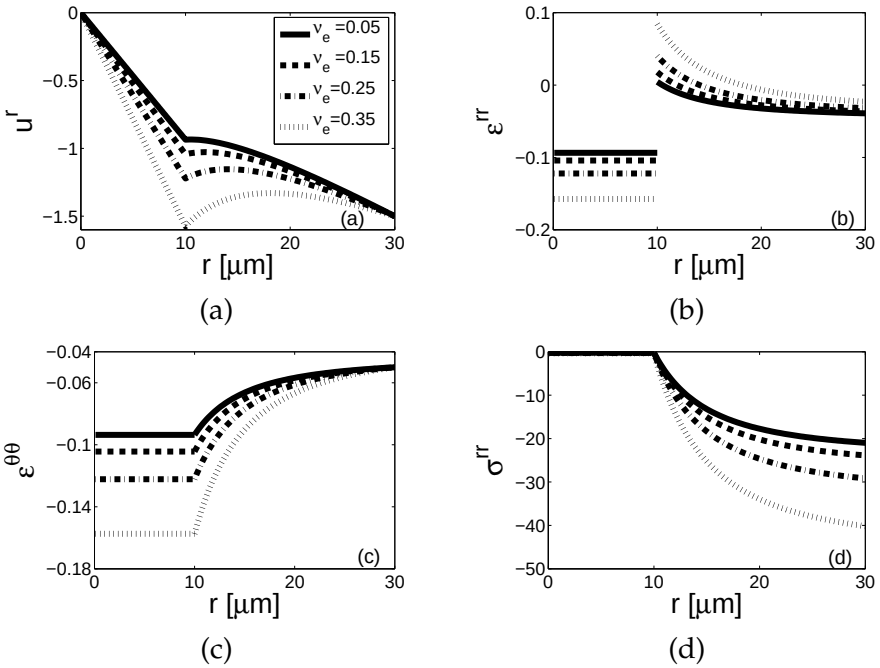

Figure 4: Analytical solutions for case 1 (Table 1) in which the Poisson's ratio (ν_e) of the extracellular region is varied in the cases $\nu_e = 0.05$ (solid), $\nu_e = 0.15$ (dashed), $\nu_e = 0.25$ (dash-dotted) and $\nu_e = 0.35$ (dotted): (a) radial displacement, (b) radial normal strain, (c) angular normal strain, (d) radial normal stress.

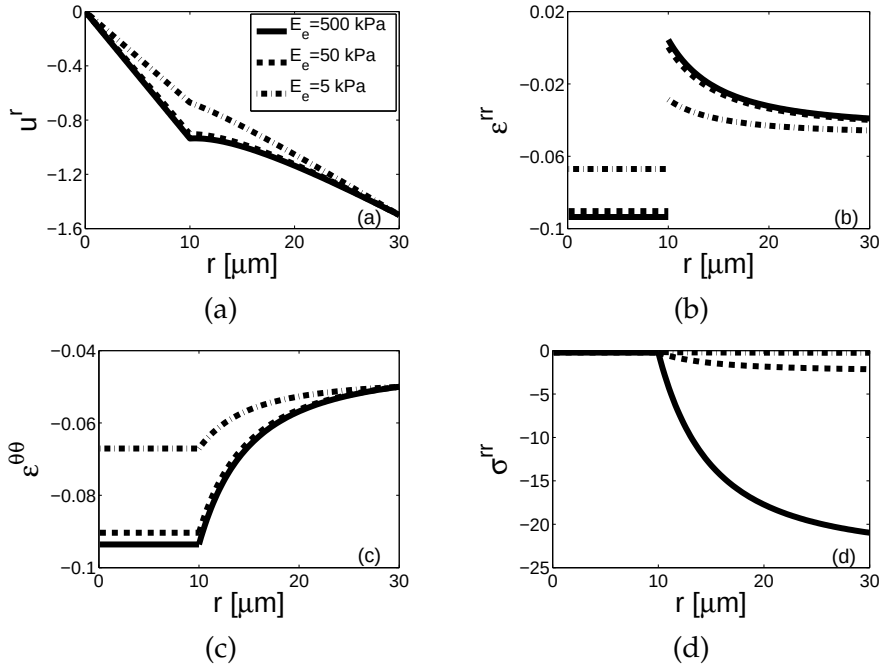

Figure 5: Analytical solutions for case 2 (Table 1) in which the Young's modulus (E_e) of the extracellular region is varied in the cases $E_e = 500$KPa (solid), $E_e = 50$KPa (dashed) and $E_e = 5$KPa (dash-dotted): (a) radial displacement, (b) radial normal strain, (c) angular normal strain, (d) radial normal stress.

Effects of parameter sensitivity on performance of the three numerical algorithms were evaluated by comparing CPU times for cases 1-3 (Fig. 6). The AMG-PCG technique exhibited significantly reduced CPU times as compared to the DS-PCG and Euclid-PCG approaches. In addition, AMG-PCG algorithm exhibited very little sensitivity to variations in material properties considered in cases 1-3, in contrast to the other two algorithms. Furthermore, CPU times for the DS-PCG and Euclid-PCG algorithms increased more dramatically than for the AMG-PCG algorithm as the DOF were increased.

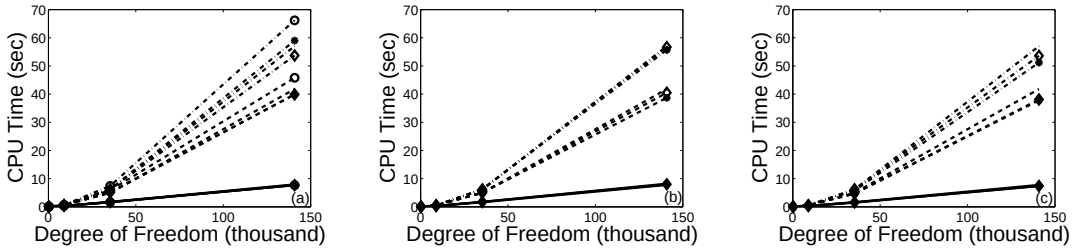

Figure 6: A comparison of CPU times for the DS-PCG algorithm (dash-dotted), the Euclid-PCG algorithm (dashed) and the AMG-PCG algorithm (solid): (a) case 1: $\nu_e = 0.05$ (no markers), $\nu_e = 0.15$ (diamonds), $\nu_e = 0.25$ (stars), and $\nu_e = 0.35$ (circles), (b) case 2: $E_e = 500$KPa (no markers), $E_e = 50$KPa (diamonds), and $E_e = 5$KPa (stars), (c) case 3: $\nu_c = 0.45$ (no markers), $\nu_c = 0.35$ (diamonds), and $\nu_c = 0.25$ (stars).

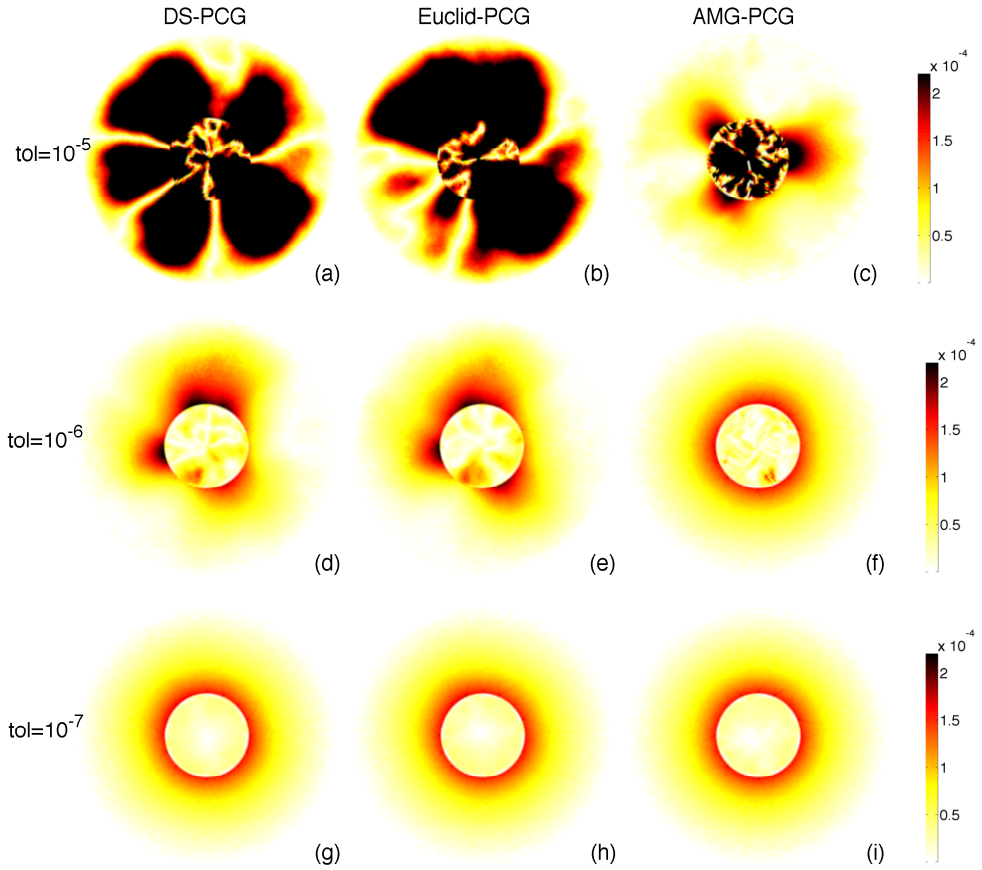

Figure 7: Absolute error of u^r for the three algorithms as the relative residual tolerance is varied.

4.3 Comparison of spatial error

Motivated by the results described above, we also evaluated spatial errors to compare the performance of the three algorithms when the tolerance was varied (case 4, Table 1) with the number of DOF set at N_3=35345. The effect of varying tolerance on CPU time is shown in Table 4, and the spatial variation of absolute errors was evaluated for the radial displacement (Fig. 7) and the radial normal strain (Fig. 8). Since our numerical FEM was formulated in polar coordinates, the radial normal strain ϵ_{rr} exhibits a singular limit as $r\to 0$ that affects its numerical accuracy and, hence, the associated strain error assessments. Consequently, in evaluating the spatial variation in error for

Table 4: Iteration counts and CPU times (seconds) as tolerance is varied (case 4) with $N_3 = 35345$.

	iteration counts			CPU time (second)		
Tol	DS-PCG	Euclid-PCG	AMG-PCG	DS-PCG	Euclid-PCG	AMG-PCG
10^{-5}	493	179	5	3.52E+0	3.22E+0	1.26E+0
10^{-6}	698	251	7	5.09E+0	4.10E+0	1.46E+0
10^{-7}	850	309	9	6.14E+0	4.59E+0	1.62E+0

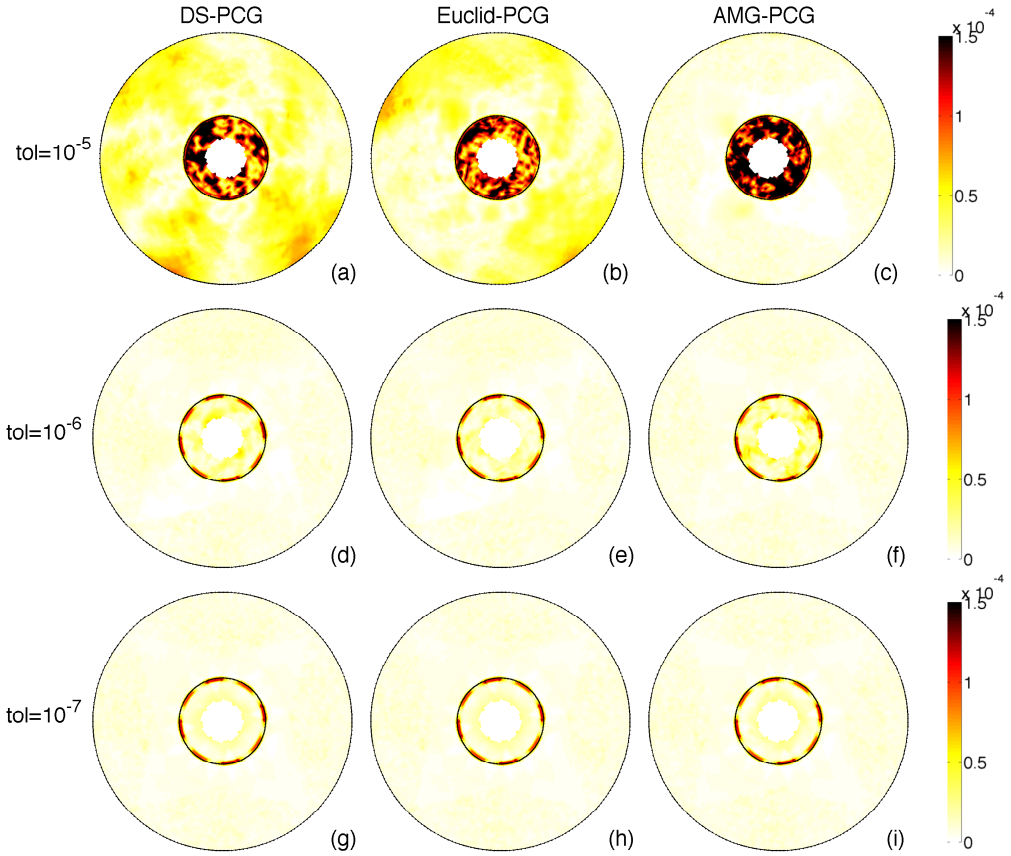

Figure 8: Absolute error of ϵ_{rr} for the three algorithms as the relative residual tolerance is varied. Boundaries of *Cell* and *ECM* are indicated by thin black lines.

ϵ_{rr}, we excluded a region of radius 4μm central to the domain containing the point r=0 (Fig. 8).

Although all three algorithms demonstrate almost identical accuracy as the relative residual tolerance is reduced to 10^{-7} (Table 3), AMG-PCG exhibits less pronounced spatial error for larger values of the relative residual tolerance. Based on the first two rows of Figs. 7(a)-(c) and Figs. 7(d)-(f), we observe that, for a fixed tolerance, displacement error for the AMG-PCG algorithm is more spatially confined to regions inside the cell and near the cell-ECM interface as compared to errors for the other two algorithms. Differences in strain error are most pronounced at the largest tolerance value (Fig. 8(a)-(c)) where error magnitudes in the ECM region are smaller for the AMG-PCG algorithm but somewhat more pronounced in the cellular region.

5 Conclusions

In this study, an analytical solution of a soft inclusion problem relevant to biomechanical deformation of cells in articular cartilage was developed and used to evaluate

iterative conjugate gradient numerical solutions of the associated linear algebraic system using algebraic multigrid preconditioning (AMG-PCG) in the context of a finite element discretization. The AMG-PCG algorithm was compared to two other preconditioning algorithms based on the use of diagonal preconditioning (DS-PCG) or a modified incomplete LU decomposition (Euclid-PCG). Overall, the AMG-PCG algorithm exhibited significant savings in CPU time with increasing number of nodal unknowns. A hallmark of successful application of MG is independence of the number of iterations on the number of DOF of the mesh, and this behavior was clearly evident in our application (Table 2). The specific MG algorithm (AMG-PCG) used in this study also exhibited little sensitivity of CPU time (Fig. 6) to variations in material properties that are known to significantly affect model variables. Evaluation of spatial error for the three algorithms (Figs. 7 and 8) demonstrates distinct convergence patterns, as well as slower convergence near the internal interface. Taken together, these findings demonstrate that the use of algebraic multigrid techniques for preconditioning iterative solution of assembled linear systems for soft elastic inclusion problems can significantly accelerate computation speed while preserving accuracy. While the current study focused on a single inclusion problem, where an analytical solution was developed for detailed evaluation of the numerical method, our results demonstrate the potential advantages of AMG-based preconditioning for the solution of larger scale problems, e.g., with many soft inclusions.

Acknowledgments

This work has been supported in part by funding from the National Science Foundation (DMS-0636590) and the National Institutes of Health (AG15768). The authors would also like to thank Dr. Zhilin Li for valuable discussions.

References

[1] A. F. BOWER, Applied Mechanics of Solids, CRC Press, 2009, Boca Raton.
[2] W. L. BRIGGS, V. E. HENSON AND S. F. MCCORMICK, A Multigrid Tutorial, 2nd Edition, SIAM, Philadelphia, 2000.
[3] Z. CHEN AND J. ZOU, *Finite element methods and their convergence for elliptic and parabolic interface problems*, Numer. Math., 79 (1998), pp. 175–202.
[4] A. J. CLEARY, R. D. FALGOUT, V. E. HENSON AND J. E. JOHNS, *Coarse grid selection for parallel algebraic multigrid*, in A. Ferriera, J. Rollin, H. Simon and S. -H. Teng, editors, Proceedings of the Fifth International Symposium on Solving Irregularly Structured Problems in Parallel, Lecture Notes in Computer Science, 1457 (1998), Springer-Verlag.
[5] J. D. ESHELBY, *The determination of the elastic field of an ellipsoidal inclusion, and related problems*, Proc. Roy. Soc. A, 241 (1957), pp. 376–396.
[6] Y. GONG, B. LI AND Z. LI, *Immersed-interface finite-element methods for elliptic interface problems with non-homogeneous jump conditions*, SIAM J. Numer. Anal., 46(1) (2008), pp. 472–495.

[7] Y. GONG AND Z. LI, *Immersed interface finite element methods for elasticity interface problems with non-homogeneous jump conditions*, Numer. Math. Theo. Meth. Appl., 3 (2010), pp. 23–39.
[8] M. GRIEBEL, D. OELTZ AND M. A. SCHWEITZER, *An algebraic multigrid method for linear elasticity*, SIAM J. Sci. Comput., 25 (2003), pp. 385–407.
[9] W. HACKBUSCH, Multi-Grid Methods and Applications, Springer-Verlag, New York, 1985.
[10] V. E. HENSON AND U. M. YANG, *BoomerAMG: a parallel algebraic multigrid solver and pre-conditioner*, Appl. Numer. Math., 41 (2002), pp. 155–177.
[11] HYPRE User's Manual, Software Version: 2.4.0b, 2008.
[12] D. HYSOME AND A. POTHEN, *A scalable parallel algorithm for incomplete factor preconditioning*, SIAM J. Sci. Comput., 22 (2001), pp. 2194–2215.
[13] M. T. JONES AND P. E. PLASSMAN, *A parallel graph coloring heuristic*, SIAM J. Sci. Comput., 14 (1983), pp. 654–669.
[14] M. LUBY, *A simple parallel algorithm for the maximal independent set problem*, SIAM J. Sci. Comput., 15 (1986), pp. 1036–1053.
[15] E. KIM, F. GUILAK AND M. A. HAIDER, *An axisymmetric boundary element model for determination of articular cartilage pericellular matrix properties in situ via inverse analysis of chondron deformation*, J. Biomech. Eng., 132 (2010), 031011.
[16] V. C. MOW, M. H. HOLMES AND W. M. LAI, *Fluid transport and mechanical properties of articular cartilage: a review*, J. Biomech., 17 (1984), pp. 377–394.
[17] Y. XIAO, P. ZHANG AND S. SHU, *Algebraic multigrid methods for elastic structures with highly discontinuous coefficients*, Math. Comput. Simul., 76 (2007), pp. 249–262.
[18] J. W. RUGE AND K. STÜBEN, *Algebraic multigrid (AMG)*, in S. F. McCormick, editor, Multigrid Methods, volume 3 of Frontiers in Applied Mathematics, 3 (1987), pp. 73–130, SIAM, Philadelphia.
[19] L. D. TREFETHEN AND D. BAU III, Numerical Linear Algebra, SIAM, Philadelphia, 1997.
[20] U. TROTTENBERG, C. W. OOSTERLEE AND A. SCHULLER, Multigrid, Academic Press, London, 2000.
[21] U. M. YANG, *Parallel algebraic multigrid methods-high performance preconditioners*, in A. M. Bruaset and A. Tveito, editors, Numerical Solution of Partial Differential Equations on Parallel Computers, pp. 209–236, Springer-Verlag, 2006.
[22] X. YANG, B. LI AND Z. LI, *The immersed interface method for elasticity problems with interfaces*, Dynam. Cont. Dis. Ser. A, 10 (2003), pp. 783–808.